Plasmonics and Magnetism in M (Mn, Cr)-Sn Codoped In_2O_3 Colloidal Nanocrystals

A thesis submitted to
Indian Institute of Science Education and Research, Pune;
in partial fulfilment of the requirements for the
BS-MS Dual Degree programme

By

ANUR YADAV
(BS-MS student, Registration No.: 20111075)

Thesis Supervisor

Dr. Angshuman Nag

Assistant Professor

Department of Chemistry, Indian Institute of Science Education and Research, Pune, India-411008

Certificate

This is to certify that this dissertation entitled "**Plasmonics and Magnetism in M (Mn, Cr)-Sn Codoped In_2O_3 Colloidal Nanocrystals**" towards the partial fulfilment of the BS-MS dual degree programme at the Indian Institute of Science Education and Research, Pune represents the research carried out by Anur Yadav at IISER Pune under the supervision of "Dr. Angshuman Nag, Assistant Professor, Department of chemistry, IISER Pune" during the academic year 2015-2016.

Date: 28/04/2016
Place: Pune

Angshuman Nag

Dr. Angshuman Nag
Assistant Professor
Department of Chemistry
IISER Pune

Declaration

I hereby declare that the matter embodied in the report entitled "**Plasmonics and Magnetism in M (Mn, Cr)-Sn Codoped In_2O_3 Colloidal Nanocrystals**" are the results of the investigations carried out by me at the Department of Chemistry, Anur Yadav, IISER Pune, under the supervision of Dr. Angshuman Nag and the same has not been submitted elsewhere for any other degree.

Anur Yadav

Date: 28-04-2016

Anur Yadav

Place: PUNE

BS-MS Dual Degree Program

ACKNOWLEGEMENTS

This thesis has been completed with the support, guidance and encouragement of numerous people. At the end of my thesis, it is my great pleasure to thank all those who had contributed in many ways to the success of this study.

I would like to express my sincere gratitude to my guide, **Dr. Angshuman Nag**, IISER Pune for providing me an incredible opportunity to carry out my 5^{th} year MS thesis project under his guidance, who has taught me to deal with scientific questions and helped me to become an independent thinker by giving his valuable advice and constant encouragement at each step of the project. I am thankful to my external supervisor **Dr. Sunil Nair**, Assistant Professor, Department of Physics, IISER Pune for his guidance and support throughout the project.

I am thankful to all my lab members especially Bharat and Pranavi for helping me throughout my project. I would like to thank my family members for being with me throughout. I am also thankful to my friend Kesava Phaneendra and the BS-MS 2011 batch people for making my IISER Pune journey memorable.

I would like to thank Dr. Sunil Nair and group for magnetic measurements and Dr. Surjeet Singh and group for electrical DC measurements. I would also like to acknowledge SAIF, IIT Bombay for ICP-OES and EPR measurements.

Table of Contents

List of Figures

List of Tables:

Abstract

Recently, localized surface plasmon resonance (LSPR) has been observed in doped semiconductor nanocrystals (NCs), with distinct differences compared to LSPR from metallic NCs. In our Sn^{4+}-doped In_2O_3 NCs, commonly known as ITO NCs, Sn^{4+} doping provides free electron in the conduction band, which in turn gives rise to LSPR. Controlling the dopant concentration allows to control carrier density, which in turn can tune the LSPR peak from near-to-mid infrared region without changing the size and shape of NCs. In addition to Sn^{4+} doping, we attempted to codope the system with magnetic ions such as Cr^{3+} and Mn^{3+}, where concentration of each dopants can be varied in the range 0-10%, and size of NCs are in the range of 7-11 nm with possibility to observe magneto-plasmonic, and magneto-electric effects in future.

Mn^{3+} precursors were used to substitute isovalent In^{3+} ions from the lattice of In_2O_3 NCs. However, after careful characterization involving powder x-ray diffraction, and Q-band EPR, the product NCs were found to be doped with Mn^{2+} ion, both in the presence and absence of Sn^{4+} codopant which suggest the conversion is happening by accumulating electrons either from oxygen vacancies. Influence of this reduction is observed in LSPR data, where both absorbance and energy of LSPR peak systematically decreases with increasing Mn content in the NCs, due to decrease in electron density which can be rationalized by electron hole recombination.

Since Mn doping decreases carrier density, we attempted to dope Cr^{3+} instead of Mn^{2+}. This is because prior electronic structure calculations shows that the unoccupied *d*-levels of Cr^{3+} are energetically higher than the conduction band minimum of In_2O_3, and therefore, electrons will not get trapped in the Cr^{3+} *d*-levels. If so, then the LSPR of Cr-Sn codoped In_2O_3 NCs should not shift with Cr^{3+} doping, and to our surprise, LSPR shifts toward higher energy with Cr^{3+} doping. Such shift towards higher energy is opposite to all other codoped systems such as Fe-Sn and Mn-Sn codoped NCs. Four probe electrical conductivity data shows increase in conductivity by increasing Cr^{3+} concentration from 1 to 10% for Cr-Sn coped In_2O_3 NCs. These electrical and plasmonic data suggest that the Cr^{3+} doping does not trap free carriers as predicted by prior theory, but the exact reason of the LSPR shifting towards higher energy is not yet clear.

1. Introduction

Localized Surface Plasmon Resonance (LSPR) is an optical phenomena which occurs when significant charge density of free electrons interacts with the incoming electromagnetic radiation, and the natural oscillation frequency of delocalized electron density comes into resonance with the frequency of irradiated electromagnetic radiation leading to enhanced light absorption and scattering.[1] The phenomenon has been extensively observed for noble metals like gold, silver, and copper in the visible region at the nanoscale with their free electron densities lying in the range of 10^{22}-10^{23}.cm^{-3}.[2-3] LSPR majorly depends on the free electron density, and it also depends slightly on factors like size of the nanoparticle, geometry and local medium.[1] Very recently, plasmonics has also been observed in degenerately doped semiconductor nanocrystals containing sufficient free carrier density. Using classical Drude model, LSPR frequency is determined by the relation:

$$\omega_{sp} = \sqrt{\frac{N_c e^2}{(\varepsilon_\infty + \varepsilon_m)\varepsilon_o m_e} - \gamma^2}$$

where ω_{sp} is the LSPR frequency, N_c is the free carrier density, e represents the electronic, charge, ε_o is the absolute permittivity of air/vacuum, ε_m is the dielectric constant of the medium, ε_∞ is the dielectric constant at high frequency when all the polarization mechanisms die out, m_e is the effective mass of the carrier and γ is the bulk collision frequency which can also be determined by measuring the linewidth in the LSPR spectrum.[1] Figure 1 shows LSPR dependence on free carrier density and doping factors. Compared to metals, plasmonics in semiconductors[4-5] is far more advantageous. In the case of metal nanoparticles, the carrier density is fixed by shape and size of nanoparticles and can't be tuned unless stringent conditions are employed to synthesize metal nanoparticles with different shapes and sizes whereas for semiconductor nanocrystals it is easily tunable by the means of doping, temperature and/or phase transitions. There have been several reports on colloidal synthesis of semiconductor nanocrystals showing tunable plasmonics in doped metal oxides.

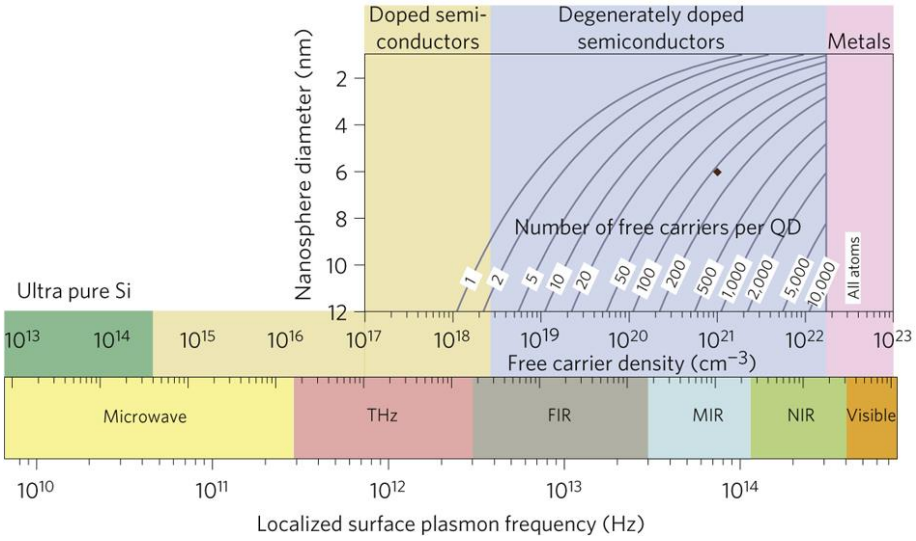

Figure 1: LSPR frequency dependence on free carrier density (adapted from reference 1 with permission of NPG).

Tin doped indium oxide known as indium tin oxide (ITO) is one of the most important doped metal oxides because of its high conductivity and transparency in visible region. Colloidal ITO nanocrystals (NCs) exhibit intense localized surface plasmon resonance (LSPR) band in the near to mid-infrared region. [6-7]

Here we dope a transition metal (Mn and Cr) in Sn^{4+} doped In_2O_3 nanocrystals (NCs),[8-9] shown in figure 1 schematic which can give rise to plasmonics and magnetism simultaneously in the same NCs.

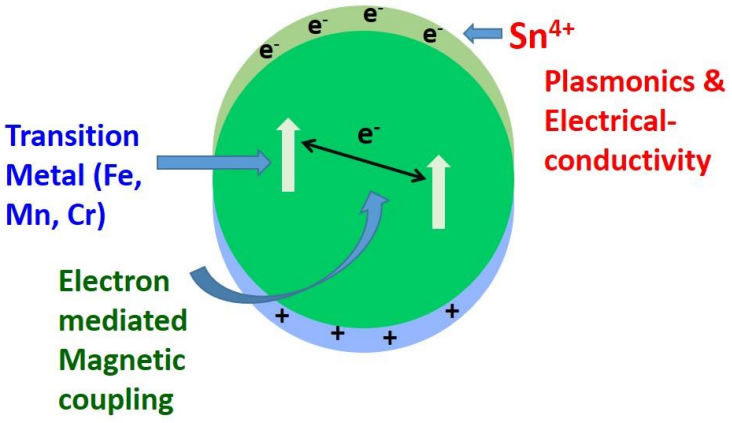

Figure 2: Schematic of transition metal doping (magnetic properties) and Sn^{4+} doping (plasmonics and conductivity).

Very recently, our group has reported Fe-Sn codoped In_2O_3 NCs which showed tunable LSPR, electrical conductivity, electron mediated magnetic coupling and visible light transparency along with solution processibility, all at the same time, but conversion of Fe^{3+} to Fe^{2+} ions reduced the extent of magnetism and created blurriness with respect to carrier mediated magnetic ordering.[8-9] We then tried another system replacing Fe^{3+} by Mn^{3+}, and it was found that in Mn-Sn codoped NCs, Mn^{3+} is converting to Mn^{2+}, i.e., on using Mn^{3+} precursors, we are getting Mn^{2+} in products and there are no Mn^{3+} ions. The presence of Mn^{2+} leads to electronic imbalance, creating hole in the NCs, which subsequently recombines with the free electron, thereby decreasing free electron density. This conversion was explained on the basis of the presence of the unoccupied Mn d states in the mid gap levels of the In_2O_3.[10]

The next obvious choice was Cr-Sn codoped In_2O_3 NCs, because prior literature shows that for Cr^{3+}, unoccupied d states lie above the conduction band minimum.[10] It was also suggested that Cr is a good candidate for long range magnetic ordering when codoped with Sn and only Cr doped In_2O_3 samples will be paramagnetic in nature.[10-11]

Both the Mn-Sn and Cr-Sn codoped NCs synthesized were found to be optically transparent in visible region and show tunable plasmonic properties with Mn and Cr doping respectively. Cr-Sn codoped In_2O_3 NCs shows unusual plasmonic properties (blue shift in plasmonic band on Cr doping) as compared to Mn-Sn codoped and also previously reported Fe-Sn codoped In_2O_3 NCs,[8-9] where LSPR dampens with Mn or Fe doping. All the Mn codoped and Cr codoped NCs exhibit non-metallic behavior in DC electrical conductivity measurements. Only Cr doped In_2O_3 NCs were found to be of paramagnetic nature as suggested by Zunger et al.[10-11]

2. METHODS

2.1. Materials:

All the chemicals used are commercially available. Indium(III) acetylacetonate (Sigma-Aldrich, purity ≥ 99.99%), Chromium(III) acetylacetonate (Sigma-Aldrich, purity > 99.99%), Mn(III) acetylacetonate (Sigma-Aldrich, purity > 99.99%) and tin(IV) bis(acetylacetonate) (Sigma-Aldrich, purity 98%), Oleylamine (Sigma-Aldrich, purity 70%), Toluene (Rankem, 99.5% purity), Methanol (Rankem, 99.9% purity).

2.2 Colloidal Synthesis of Mn-Sn and Cr-Sn codoped Nanocrystals (NCs):

The colloidal Mn-Sn and Cr-Sn codoped In_2O_3 nanocrystals (NCs) were synthesized through simple single-step strategy synthesis as used for Fe and Sn doped In_2O_3 NCs.[8-9] Indium(III) acetylacetonate, Manganese(III) acetylacetonate, Chromium(III) acetylacetonate and tin(IV) bis(acetylacetonate) dichloride were the precursors used for In_2O_3, Mn, Cr and Sn doping respectively. The stoichiometric amounts of these precursors were taken to synthesize the target composition of the nanocrystals. As an example, to prepare 10% Cr and 10% Sn codoped In_2O_3 NCs at the scale 500mg, 1.21 mmol of In, 0.151 mmol of Cr, and 0.151 mmol of Sn precursors were mixed with 10 mL of oleylamine in a 50 mL three-necked round-bottom flask. First, the reaction mixture was degassed at room temperature for 20 min in N_2 atmosphere and vacuum conditions alternatively, and then temperature was increased to 100 ºC under vacuum and was kept for 30 min. The temperature of the reaction mixture was then increased to 220 ºC under N_2 atmosphere and the reaction was kept undisturbed for 5 hrs. After the completion of the reaction, the solution was cooled to room temperature and 30 mL of methanol is added as a non-solvent in order to precipitate the NCs, followed by centrifugation at 6000 rpm for 7 min. The NCs obtained were redispersed in 10 mL of toluene and were again precipitated using 10 mL of methanol as a non-solvent, and the process was repeated twice in order to remove excess of oleylamine. The obtained oleylamine capped NCs can be dissolved in suitable non-polar solvents like tetrachloroethylene, toluene and chloroform to study their different characteristic properties. The color of the nanocrystals depends on the type and extent of doping (figure 3).[8-9]

Figure 3: Photograph of the reaction mixture of the colloidal NCs a) 10% Mn doped In_2O_3 NCs showing reddish color, b) 10% Cr-10% Sn codoped In_2O_3 NCs showing intense bluish green color.

2.3 Characterization and Measurements:

Elemental analysis of the NCs were done by Energy Dispersive X-Ray Analysis (EDAX), which was obtained using Zeiss Ultra Plus Scanning Electron Microscopy measurement and Inductively Coupled Plasma - Optical Emission Spectrometry (ICP-OES), which was done using Perkin-Elmer Optima 7000 DV machine. UV-vis-NIR absorption spectra of NCs were obtained using PerkinElmer, Lambda-950 UV/vis spectrometer and Shimadzu UV-3600 Plus UV-Vis-NIR spectrophotometer after dissolving wet sample in tetrachloroethylene (TCE) solvent. Powder X-ray Diffraction (XRD) patterns of the NCs were measured using a Bruker D8 Advance X-ray diffractometer using Cu Kα (1.54 Å) as X-ray source. Transmission Electron Microscopy (TEM). Magnetic measurements were done using SQUID magnetometer (Quantum Design MPMS XL-7 Magnetometer). Zero-Field-Cooled (ZFC) and Field-Cooled (FC) measurements were done in the temperature range of 2-300 K at magnetic field, H = 100 Oe after cooling the samples in zero-field and 100 Oe field, respectively. Electrical Resistivity were done using the AC Transport Measurement system (ACT) (Quantum Design PPMS Evercool-II).

3. Results and Discussions

3.1. Mn-Sn codoped In_2O_3 NCs

3.1.1. Elemental Analysis

Elemental analysis has been done by Inductively Coupled Plasma - Optical Emission Spectrometry (ICP-OES) and Energy Dispersive X-Ray Analysis (EDAX). It has been shown in Table 1 that for all compositions, ratio of In : Mn : Sn measured by both ICP-OES and EDAX gives similar results as compared to precursor ratios. These results shows the high efficiency of doping of Mn and Sn in In_2O_3 NCs, which was reported earlier in similar systems when precursors with pre-bonded metal-oxygen moieties (Mn-O, Sn-O and In-O) were used.[8-9]

In:Mn:Sn		
Precursor Ratio	EDAX analysis	ICP-OES
95:5:0	95.5:4.5:0	95.5:4.5:0
85:10:5	87.3:8.3:4.5	
85:5:10	84.1:5.5:10.4	88.8:4.4:6.8
89:1:10	90.2:0.8:9.0	
99:1:0	98.9:1.1:0	99.1:0.9:0
90:10:0	91.3:8.7:0	
80:10:10	83.8:8.1:8.1	
90:5:5		91.8:4.56:3.6

Table 1: Elemental analysis of Mn-Sn codoped In_2O_3 NCs using ICP-OES and EDAX.

3.1.2. Structural and Morphological studies

Powder X-ray diffraction (XRD) was done for varying amounts of Mn and Sn dopants shown in figure 4a and 4b. The XRD patterns of all the doped NCs match with that of the undoped In_2O_3 NCs and bulk In_2O_3 (JCPDS 88-2160) having cubic bixbyite structure - space group *Ia3*, 206. The absence of the impurity peak suggests formation of phase pure samples.

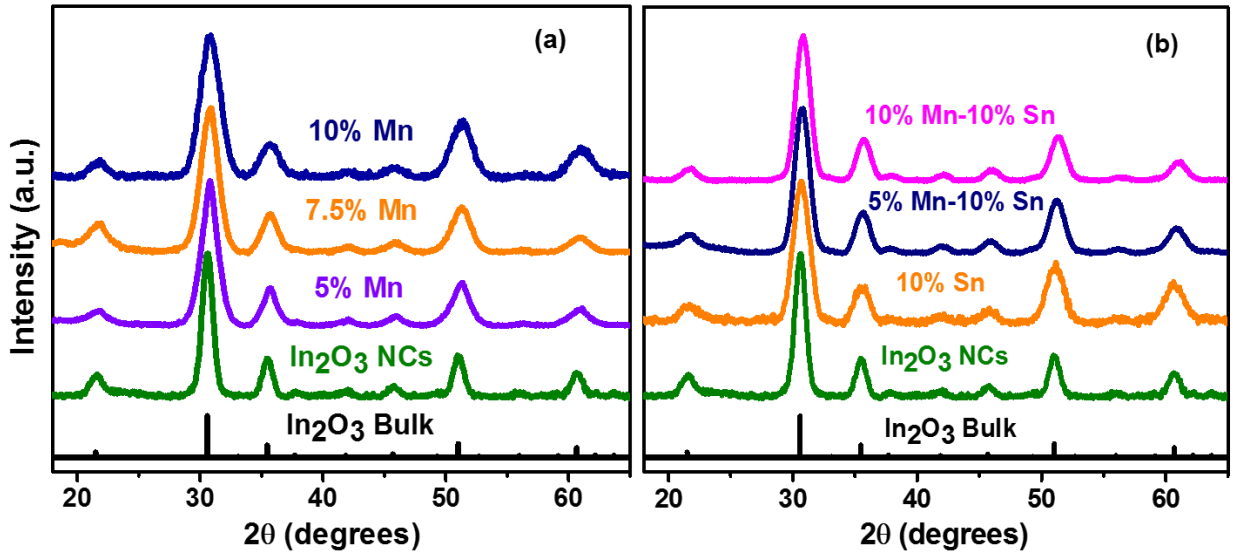

Figure 4: XRD pattern for a) % Mn doped In_2O_3 NCs. b) % Mn-10% Sn codoped In_2O_3 NCs.

In case of Mn doped In_2O_3 NCs, Mn doping causes a shift in 2θ towards higher angles systematically i.e., decrease in interplanar distance, which can be explained by the difference in the effective ionic radii of In^{3+} (0.79 Å) and Mn^{3+} (0.65 Å) as per Braggs Law of diffraction.[12] While, in powder XRD patterns of Mn-Sn codoped In_2O_3 NCs, it was observed that there is no shift in 2θ value of XRD peak for 10% Sn doped In_2O_3 NCs as compared to in bulk In_2O_3 and hence, has similar lattice parameters which is consistent with previous literature studies.[15] In case of 5% Mn-10% Sn and 10% Mn-10% Sn codoped In_2O_3 NCs, 2θ value shifts towards higher angles systematically, i.e., the lattice parameter decreases.

The decrease in lattice parameter on Mn doping can be explained by the difference in the effective ionic radii of In^{3+} (0.79 Å) and Mn^{3+} (0.65 Å), but the prior literature shows that the decrease in lattice constant has been found for both Mn^{2+} (r_{eff} = 0.82 Å) as well as Mn^{3+} doping, which suggests a complex interplay may be in place.[13-14] There may be the

possibility of the presence of Mn^{2+} due to high redox potential of Mn^{3+}/Mn^{2+} conversion (1.51 V).[16] These electrons for conversion can come from either oxygen vacancies or by Sn codoping.[17]

Transmission electron microscopy (TEM) was done for 10% Mn-10% Sn codoped In_2O_3 NCs (Figure 5). It was observed that all NCs are nearly spherical and similar in size. Also average size of the nanocrystals is ~ 6-7nm, which matches with the size calculated by using Debye-Scherrer equation. High Resolution (HRTEM) image in figure 5b shows interplanar distance of 2.85 Å and 2.54 Å which corresponds to the (222) and (400) planes respectively and agrees well with the value calculated from XRD peak using Bragg's equation. The d(222) values for the undoped In_2O_3 NCs and 10% Sn doped In_2O_3 NCs are 1.93 and 1.94 respectively, therefore decrease in interplanar distance on Mn doping further confirms that Mn and Sn has been doped in the lattice.

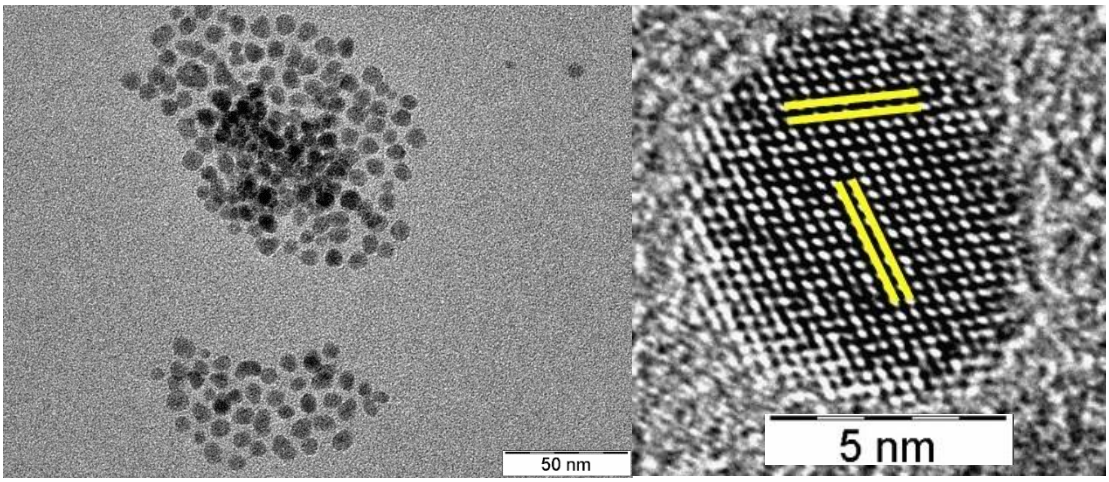

Figure 5: a) TEM image b) HRTEM image of 10% Mn-10% Sn codoped In_2O_3 NCs.

3.1.3. Electron Paramagnetic Resonance (EPR)

In order to probe the oxidation state of Mn in doped In_2O_3 NCs, Q band EPR was done. Figure 6 shows the Q Band EPR spectra for Mn doped In_2O_3 NCs and Mn-Sn codoped In_2O_3 NCs. The spectrum for each case shows an EPR signal having six hyperfine lines centered at around g = 2.003, which is the characteristic feature of Mn^{2+}. Mn^{2+} being a d^5 system readily gives EPR due to the formation of Kramer's doublets. It has 3 Kramer's doublets i.e. ±1/2, ±3/2, ±5/2 which gives rise to 6 transitions and hence 6 hyperfine

splitting lines of EPR signal.[18] It is important to note here that Mn^{3+} is a d^4 system having integer spin value = 2, and belongs to non-kramer category. Q band (35 GHz) is a high field high frequency EPR (HFEPR), which is used in measurements of complexes having non-kramers which are X band (9.35 GHz) EPR silent, due to high zero field splitting energy. So, in Q band EPR, Mn^{3+} is also supposed to give EPR signal centered at around g=2.21 and since there is no evidence of the presence of Mn^{3+} ions in the EPR spectra, so no possibility of the presence of Mn^{3+} ions in the NCs.[18]

This confirms that in product, Mn^{2+} is present in both 1% Mn doped as well as 1% Mn-10% Sn codoped In_2O_3 NCs even on using Mn^{3+} precursors. Here, Mn^{3+} ions are reduced to Mn^{2+} ions both in absence as well as in presence of Sn^{4+}. It may be the case that oxygen vacancies in the NCs act as electron donor and thereby reducing Mn^{3+} to Mn^{2+}.[17]

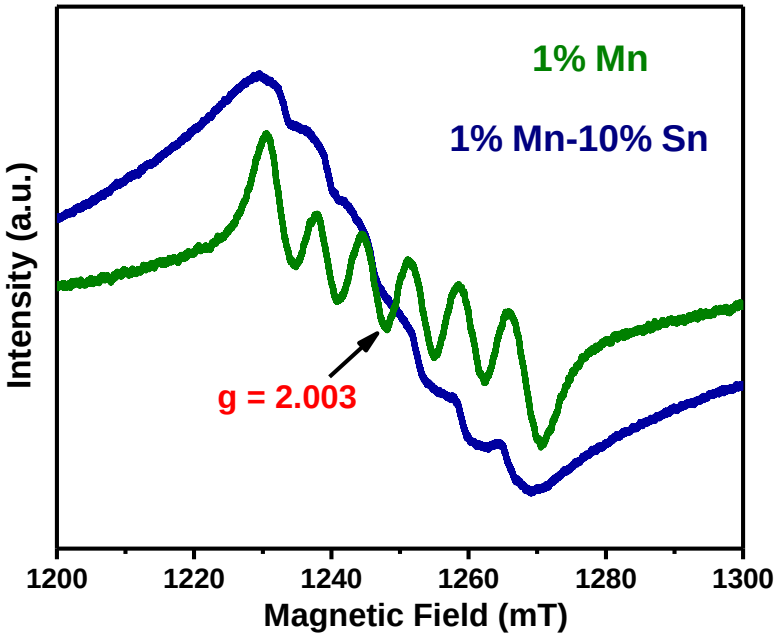

Figure 6: Q band EPR spectra of 1% Mn doped and 1% Mn-10% Sn codoped In_2O_3 NCs.

The hyperfine splitting constant for 1% Mn doped and 1% Mn-Sn codoped NCs lies between 7.1 to 7.4 mT and is similar to the other Mn^{2+} doped in bulk oxides. This suggests significant covalent character of Mn-O bonds, which also act as a proof of Mn doping in the lattice of our NCs.[19-20]

The conversion of Mn^{3+} to Mn^{2+} can be explained by the theoretical model proposed by Zunger et al.[10] shown in figure 7 (adapted from reference 10 by permission of APS), where theoretical calculations regarding formation of 3d defect levels for 3d transition metal substituting In^{3+} in In_2O_3 host lattice has been done. They described the electronic structure in terms of single particle energy levels(*e*-,*t*-,*e*+ and *t*+) , which form hybrids known as crystal field resonances (CFRs). In In_2O_3 lattice, there are two substitution sites, *b* and *d*, both of which are nearly in octahedral symmetry. In octahedral symmetry of lattice sites, the *d* levels of 3d dopant gets split into sets of *t* and *g* levels where the spin configuration further splits them into t_+, e_+, t_- and e_- levels. In case of Mn^{3+}, the highest occupied level (e_+) lies in between the host band gap which undergoes jahn teller distortion due to partial occupancy, creating fully occupied (HOMO) and empty levels (LUMO). This LUMO lies very close to the conduction band (C.B.) minimum and act as acceptor state. The electrons provided by oxygen vacancies will form a shallow band near the CBM and will act as donor level.[17] The interaction between these acceptor and donor levels will result in complete filling of e_+ level, converting Mn^{3+} to Mn^{2+}. This is the reason of obtaining Mn^{2+} in products even on using Mn^{3+} precursor.

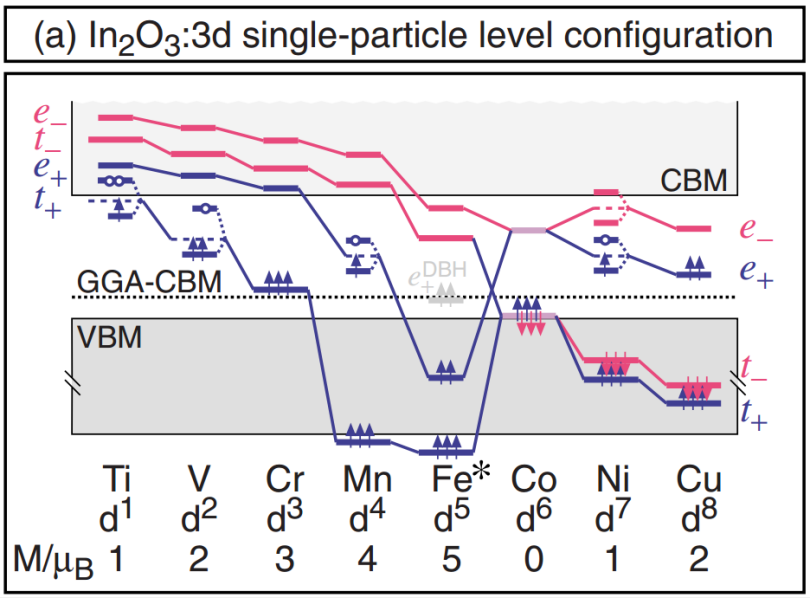

Figure 7: a) Single particle energy levels for 3d impurities in In_2O_3, showing “crystal field resonances” (CFRs) levels in blue and red color. (adapted from reference 10 with permission from APS).

However, oxygen vacancy concentration in undoped In_2O_3 NCs is usually very low, i.e., less than 0.5% of the total oxygen concentration[17], so ideally, in only Mn doped In_2O_3 NCs, the number of electrons released by creation of oxygen vacancies won't suffice for the conversion of all Mn^{3+} to Mn^{2+} with charge imbalance further complexing the scenario. However, previous literature has suggested that Mn^{2+} doping in In_2O_3 is usually assisted with creation of oxygen vacancies[14] following equation:

$$2In_{In}^{x} \rightarrow 2In_{Mn}^{'} + V_{O}^{\cdot\cdot}$$

which means that substitution of In atoms at an In site (neutral charge on the site denoted by x) with a Mn^{2+} ion leaves a negative charge (') on the In site which is balanced by creation of an oxygen vacancy leaving +2 positive (˙) charge. This creation of new oxygen vacancies facilitate conversion of other Mn^{3+} ions to Mn^{2+}.

3.1.4. UV-Vis-Near Infrared Absorption

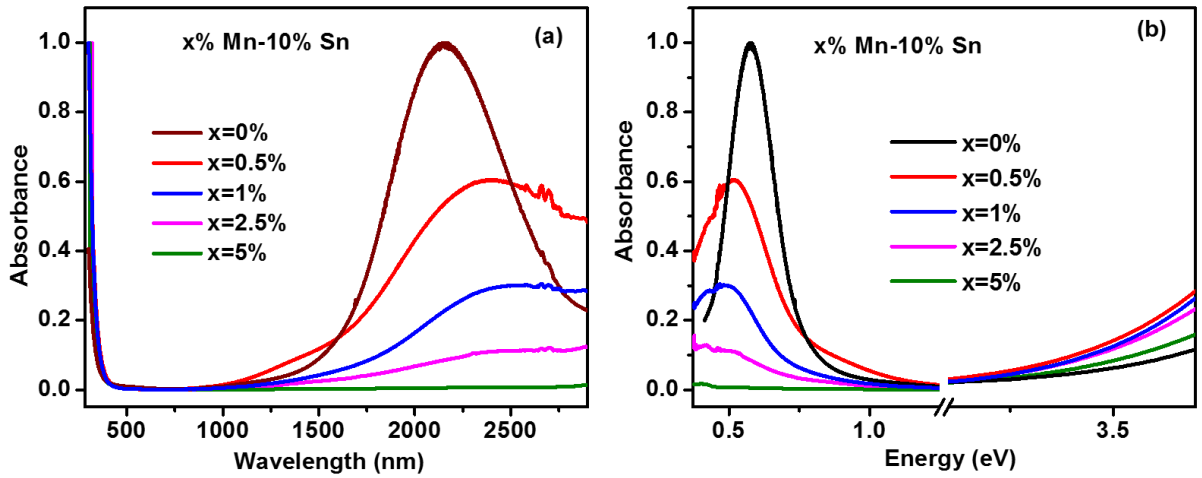

Figure 8: Mn-Sn codoped In_2O_3 NCs showing LSPR band a) in wavelength scale b) in energy scale.

On doping Sn^{4+} in the lattice of In_2O_3 NCs, a delocalized free electron is generated in the conduction band, which on interaction with electromagnetic radiation exhibits an intense localized surface plasmon resonance (LSPR) band at 2150 nm (0.577 eV) [23-24] shown in figure 8a and 8b. The 10% Sn doped In_2O_3 NCs are transparent in visible region showing an additional peak corresponding to optical band gap transition in UV region. The optical band decreases with Mn codoping because of sp-d exchange interaction.[25]

The LSPR band absorbance and peak energy dampens systematically with Mn codoping and disappears at 5% Mn codoping. The LSPR band depends on size, shape, refractive index of the medium and carrier density.[1] Since all the NCs are spherical in shape with size of 6-7nm and refractive index of the medium (tetrachloroethylene) remains same, the decrease in LSPR is rationalized by the decrease in delocalized electron density in conduction band (CB).

The decrease in CB delocalized electron density can be because of the following reasons:

(1) presence of Mn^{2+} (Indium is in 3+ oxidation state) will result in formation of a hole which will act as free electron scavengers by causing electron hole recombination, which is shown by the following equations:

$$In^{3+} \rightarrow Sn^{4+} + e^{-}$$

$$In^{3+} \rightarrow Mn^{2+} + h^{+}$$

$$2In^{3+} \rightarrow Sn^{4+} + Mn^{2+}$$

Here, first equation shows an extra electron on doping with Sn^{4+}, second equation shows the formation of hole on doping with Mn^{2+}. Equation three is a combination of first and second, which shows that no electrons are left when two In^{3+} ions are substituted, each with one Sn^{4+} and one Mn^{2+}.

(2) increase in electron scattering with increase in Mn ions which is also suggested by increase in Half width at half maxima (HWHM) with Mn doping (figure 9).

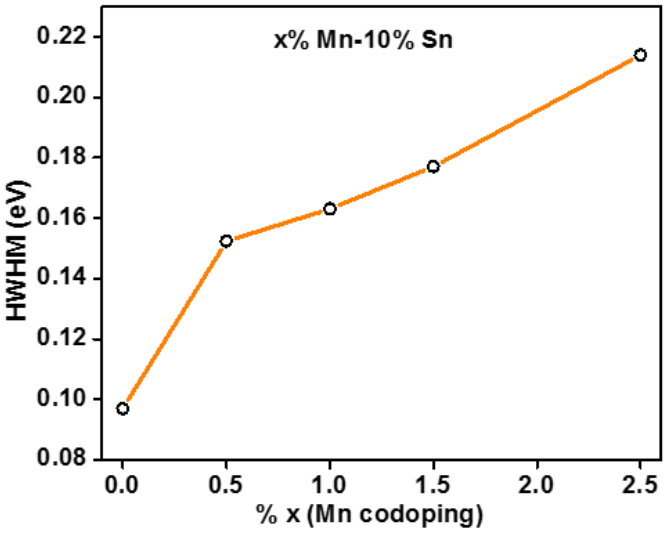

.

Figure 9: variation in HWHM of Mn-Sn codoped In_2O_3 NCs with % Mn codoping.

3.1.5. Electrical DC and AC Measurements

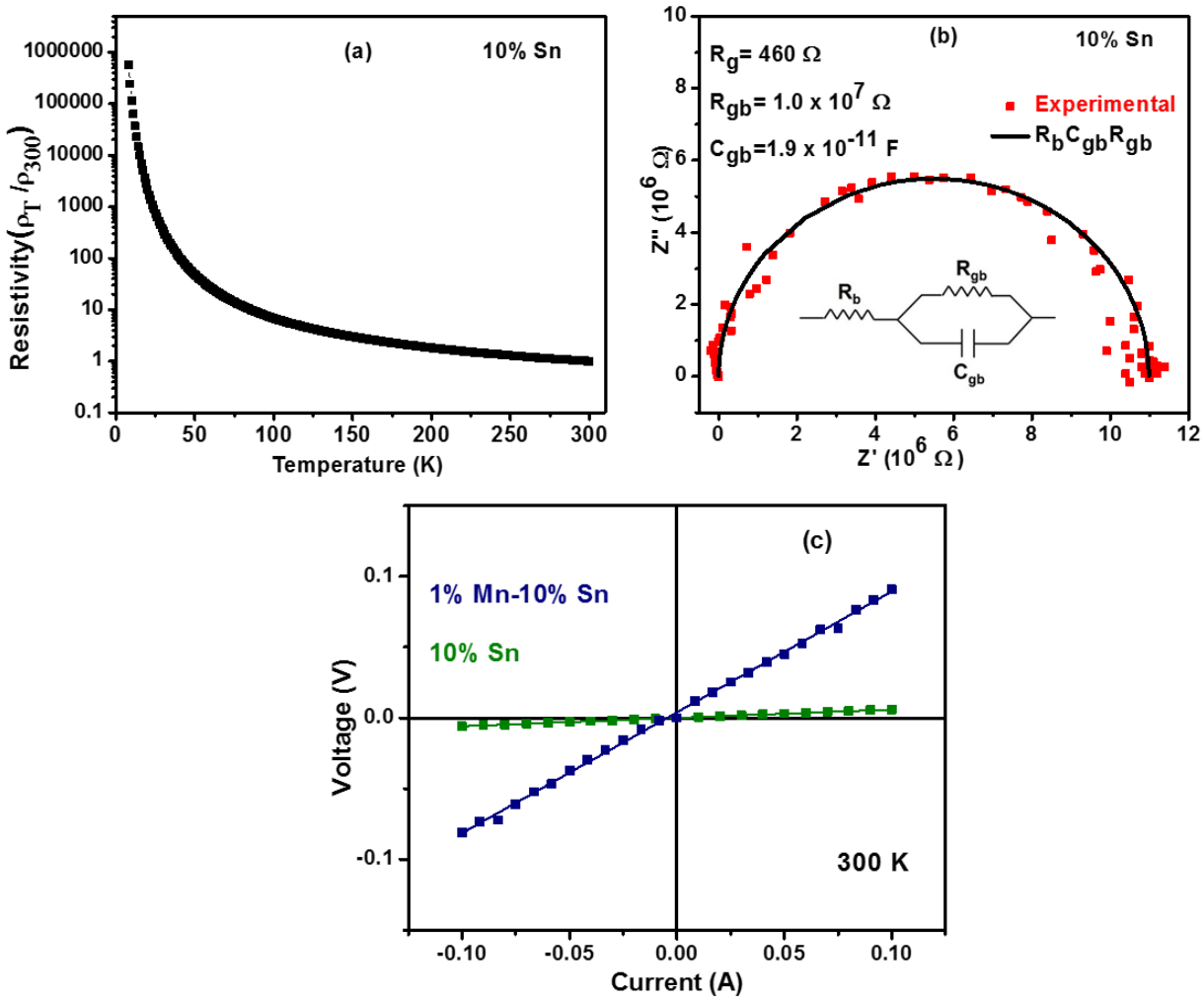

Figure 10: 10% Sn doped In_2O_3 NCs showing a) Temperature dependent resistivity plot showin non-metallic behavior where ρ_T is resistivity at any temperature and ρ_{300} is resistivity at 300K b) Nyquist plot of AC Impedance measurements showing grain boundary dominance in DC electrical measurements. c) voltage vs current graph showing linear ohmic relationship for 10% Sn and 1% Mn-10% Sn codoped In_2O_3 NCs, and decrease in resistance on Mn codoping.

Four-probe DC electrical measurement was done for all Mn-Sn codoped In_2O_3 NCs on solid pellets. In figure 10a, resistivity dependence on temperature plot is shown for 10% Sn doped In_2O_3 NCs. Resistivity of the NCs decreases with increasing temperature, and therefore, our sample exhibits a typical non-metallic behavior shown in figure 10b. Such

behavior was shown by all doped and undoped NCs. Also, figure 10c shows that NCs follow a linear ohmic relationship and resistivity increases with increasing Mn dopant concentration, which can be attributed to the decrease in the conduction band delocalized electrons. This decrease in electrical conductivity further supports decrease in electron density on codoping with Mn. The non-metallic behavior shown by our NCs can be due to extensive contribution from the grain boundary [21] and AC measurements were done in order to confirm.

Two-probe AC impedance of NC film of 10% Sn codoped In_2O_3 (figure 10b) was measured in order to separate the contribution from intra-grain (intra-NC) and grain boundary. A typical semicircular nyquist plot is obtained for AC impedance of polycrystalline NCs.[22]The experimental data was fitted using $R_gR_{gb}C_{gb}$ electrical circuit also shown in the figure 10b, where C_{gb} (capacitance across grain boundary) is connected in parallel to Rgb (resistance across the grain boundary), whose resultant is in series with R_g (resistance within the grain boundary). The obtained parameters after fitting for 1% Mn-10% Sn codoped In_2O_3 NCs are R_g = 460 Ω, R_{gb} = 10^7 Ω, and C_{gb} = 19 pF. A capacitance of 19 pF is similar to the expected values across grain boundary of a polycrystalline material.[22]

We can clearly see that there is a huge difference between the values of R_g and R_{gb}, i.e., contribution from grain boundary dominates over an individual grain. This means that an electron may be delocalized within a grain but at the interface of two grains becomes localized.

3.1.6. Magnetism

From EPR data, it was confirmed that Mn is present in oxidation state of +2. So, magnetic measurements of samples obtained with Mn(III) precursor were not carried out. Instead, in parallel with this work, Mn(II)-Sn codoped In_2O_3 NCs were synthesized from Mn^{2+} precursors in collaboration with Bharat Tandon, which were found to exhibit carrier mediated magnetic ordering (Figure 11) and will be dicussed in detail in his PhD thesis.

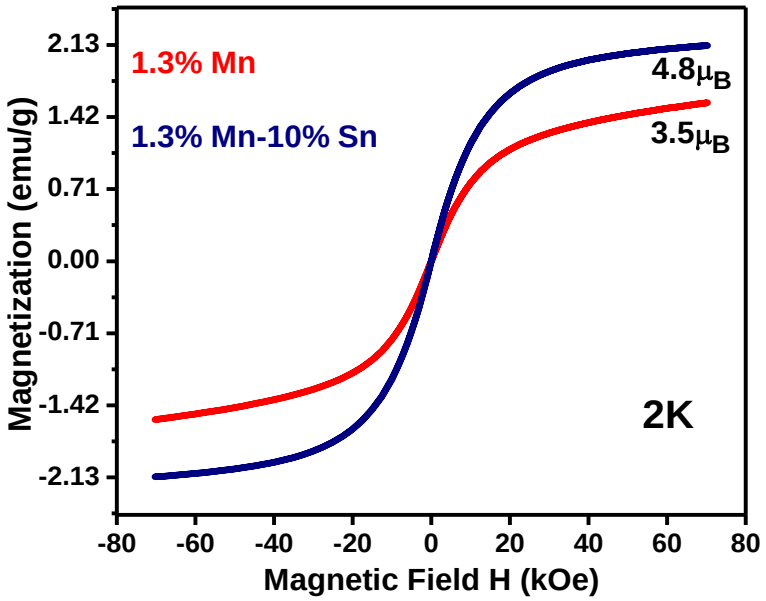

Figure 11: Comparison between and 1.3% Mn(II) doped and 1.3% Mn(II)-10% Sn codoped In_2O_3 NCs in order to establish claim of the electro mediated magnetic coupling. This work has been done in collaboration with Bharat Tandon and will be discussed in detail in his PhD Thesis.

3.2. Cr-Sn codoped In_2O_3 NCs

Even on showing several interesting properties like tunable plasmonics and precursor independent oxidation state, there were several drawbacks of the Mn-Sn codoped In_2O_3 NCs like unstability of the +3 oxidation state of Mn in NC products and decrease in electron density of 10% Sn doped In_2O_3 NCs on codoping with Mn. In order to overcome these problems, a new system, "Cr-Sn codoped In_2O_3 NCs" was chosen based on the theoretical studies done by Zunger et. al. which shows that for Cr^{3+}, unoccupied 3d levels are energetically higher than the conduction band minimum of In_2O_3, and therefore, electrons will not get trapped in the Cr^{3+} *d*-levels.

It was also suggested that Cr is a good candidate for long range magnetic ordering when codoped with Sn, because of the partial occupancy of 3d levels which results in energetically favorable interaction between Cr spins and only Cr doped In_2O_3 samples will be paramagnetic in nature.[10-11]

3.2.1. Elemental Analysis

Elemental analysis of the Cr doped and Cr-Sn codoped In_2O_3 NCs samples has been done by ICP-OES and EDAX. EDAX gives X-Ray emission spectrum, in which peaks of each element can be detected based on the X-Ray energy emitted corresponding to their unique atomic structure.

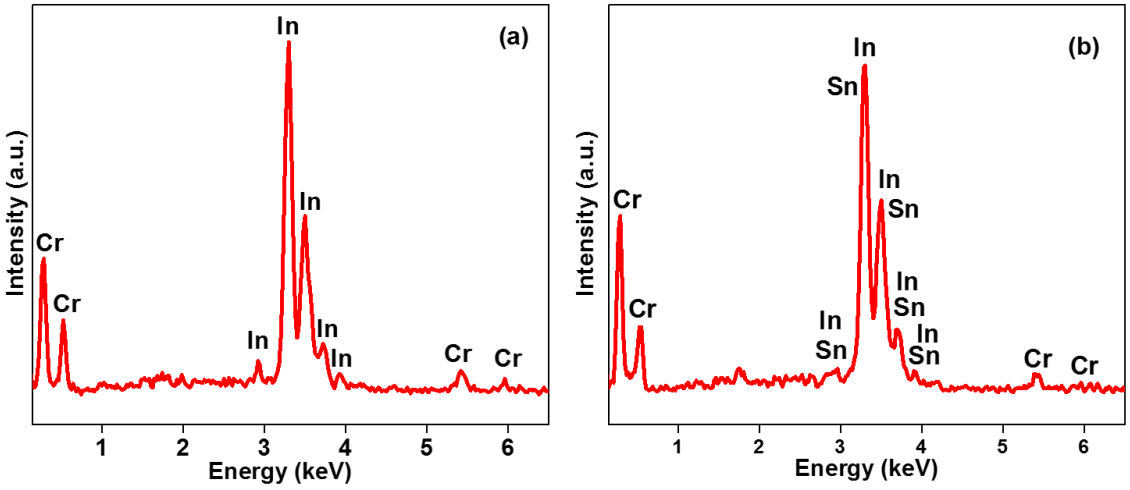

Figure 12: EDAX spectra of a) 10% Cr doped In_2O_3 NCs and b) 10% Cr-10% Sn codoped In_2O_3 NCs.

For example 10% Cr doped In_2O_3 NCs EDAX spectrum shown in figure 12a shows the peaks corresponding to Cr and In. While EDAX spectra in figure 12b for 10% Cr-10% Sn codoped In_2O_3 NCs shows the peaks corresponding to Cr, Sn and In. The peaks of In and Sn overlaps with each other due to similar atomic numbers, i.e., In and Sn will show peaks at similar energies.

It has been shown in Table 2 that for all compositions where Cr and Sn doping concentrations were varied in the range of 0-10%, molar ratio of In : Cr : Sn measured by both ICP-OES and EDAX gives similar results as compared to precursor ratios. These results shows the high level of doping of Cr and Sn in In_2O_3 NCs, which was reported earlier in similar systems when precursors with pre-bonded metal-oxygen moieties (Cr-O, Sn-O and In-O) were used.[8-9] For all further discussions, precursor ratios will be used throughout the thesis.

In : Cr : Sn		
Precursor Ratio	EDAX Analysis	ICP-OES Analysis
99 : 1 : 0	98.8 : 1.2 : 0	98.8 : 1.2 : 0
89 : 1: 10	87.9 : 1.3 : 10.8	
95 : 5 : 0	95 : 4.7 : 0	94.5 : 5.5 : 0
85 : 5 : 10	85.8 : 4.1 :10.1	
90 : 10 : 0	90.2 : 9.8 : 0	88.3 : 11.7 : 0
80 : 10 : 10	80.6 : 8.3 : 11.1	

Table 2: Elemental analysis of Cr-Sn codoped In_2O_3 NCs using ICP-OES and EDAX

3.2.2. Structural and Morphological Studies

The powder XRD patterns of all the Cr doped (figure 13a) and Cr-Sn codoped (figure 13b) NCs matches with that of the In_2O_3 NCs and bulk In_2O_3 (JCPDS 88-2160) corresponding to the cubic bixbyite structure - space group Ia3, 206. The absence of the impurity peaks suggest formation of phase pure samples. On doping with Cr, there was a clear shift in the peaks to higher angles, and it shifts further at higher concentrations of Cr. This was

observed in both Cr doped and Cr-Sn codoped In_2O_3 NCs. The shift towards larger 2θ value indicates a reduction in the lattice constant with Cr doping which is expected since the smaller Cr^{3+}(R_{eff} = 0.62Å) ions are replacing In^{3+}(R_{eff} = 0.79Å) ions in the In_2O_3 lattice as per Braggs law of diffraction.[12] The lattice constant decreases from 10.108 Å (undoped In_2O_3) to 10.037 Å for 5% Cr doped In_2O_3.[26] Similarly, it also decreases for Cr-Sn codoped NCs from 10.084 Å (10% Sn doped In_2O_3) to 10.069 Å (10% Cr-10% Sn doped In_2O_3). So, from XRD results, it can be concluded that Cr and Sn has been doped in the In_2O_3 lattice

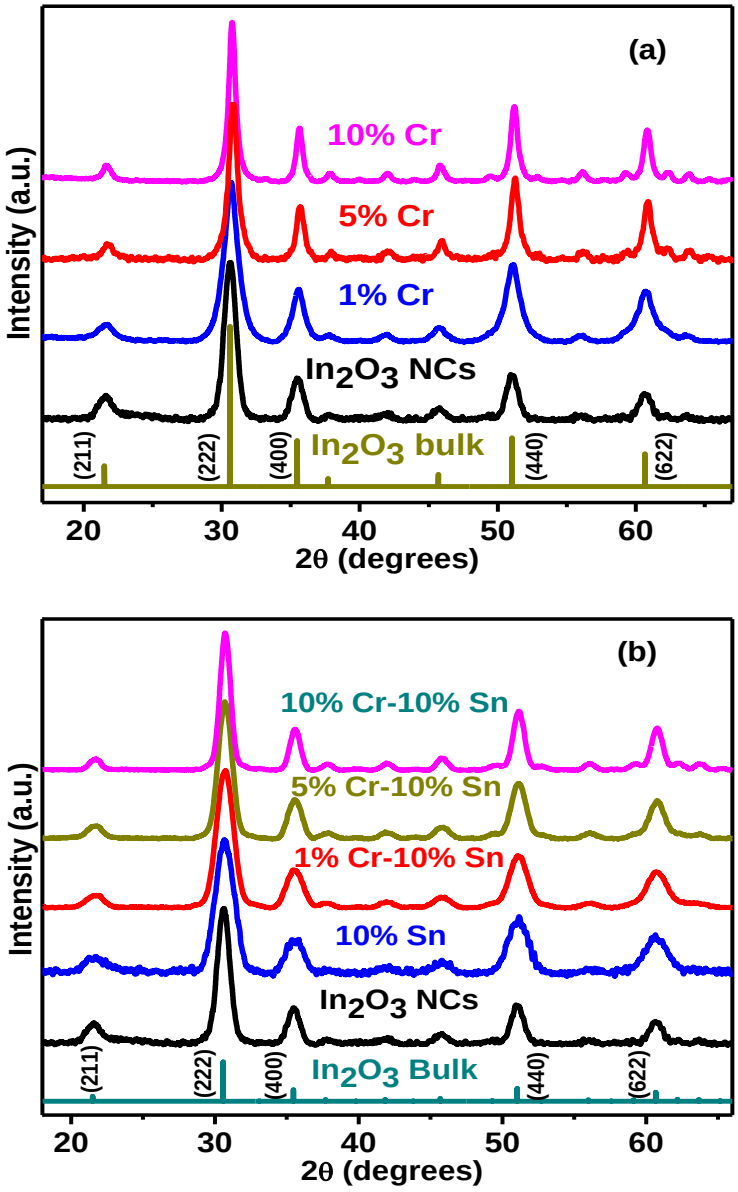

Figure 13: a) XRD pattern a) Cr doped In_2O_3 NCs. b) Cr-Sn codoped In_2O_3 NCs.

Furthermore, size of the nanocrystals or crystallite size was calculated from debye-scherrer equation (table 3) which gives an approximate estimation of the size. The equation is given by:

$$\tau = \frac{\mathbf{K}\,\lambda}{\beta \cos\theta}$$

where K = dimensionless shape factor, with a value of 0.9

β = line broadening at half the maximum intensity (FWHM), Δ(2θ).

λ = X-Ray wavelength (1.54 Å), θ = Braggs angle.

Sample Description	**Interplanar distance d(400) (Å)**	**Size τ (nm)**
In_2O_3	2.529	7.6
1% Cr doped In_2O_3	2.520	8.4
5% Cr doped In_2O_3	2.514	11.8
10% Cr doped In_2O_3	2.517	15.1
10% Sn doped In_2O_3	2.524	5.3
1% Cr-10% Sn codoped In_2O_3	2.523	6.0
5% Cr-10% Sn codoped In_2O_3	2.521	7.5
10% Cr-10% Sn codoped In_2O_3	2.519	9.7

Table 3: Interplanar distance ‘d’ calculated from Braggs equation and size calculated from debye-scherrer equation for the NCs.

It was found that crystallite size increases with Cr doping in both Cr doped as well as Cr-Sn codoped NCs. This can also be seen in XRD peaks, as the peak becomes narrow (FWHM decreases) the crystallite size increases.

Transmission Electron Microscopy (TEM) technique gives the information about the shape and size of the NCs. TEM image shown in figure 14 exhibit nearly spherical shape

and similar size of NCs. Similarly, Cr-Sn codoped NCs in figure 15(a), (b) and (c) also follows the same characteristic properties. Figure 14 and Figure 15 also shows size histograms with gaussian curve of good monodispersity with average diameters ranging from 6.5 to 10.5nm. The average diameter of 1% Cr doped and 10% Cr doped NCs are 5.6 nm and 8.5 nm respectively. While the average diameter of 1% Cr- 10% Cr, 5% Cr-10% Cr and 1% Cr- 10% Cr codoped In_2O_3 NCs are 6.5 nm, 8.4 nm and 10.2 nm respectively. All the NC's diameter matches well with the sizes determined from XRD (debye-scherrer equation) results in table 3. It can be clearly seen in figure 15 that size histogram is shifting towards larger size as Cr concentration is increasing in Cr-Sn codoped NCs.

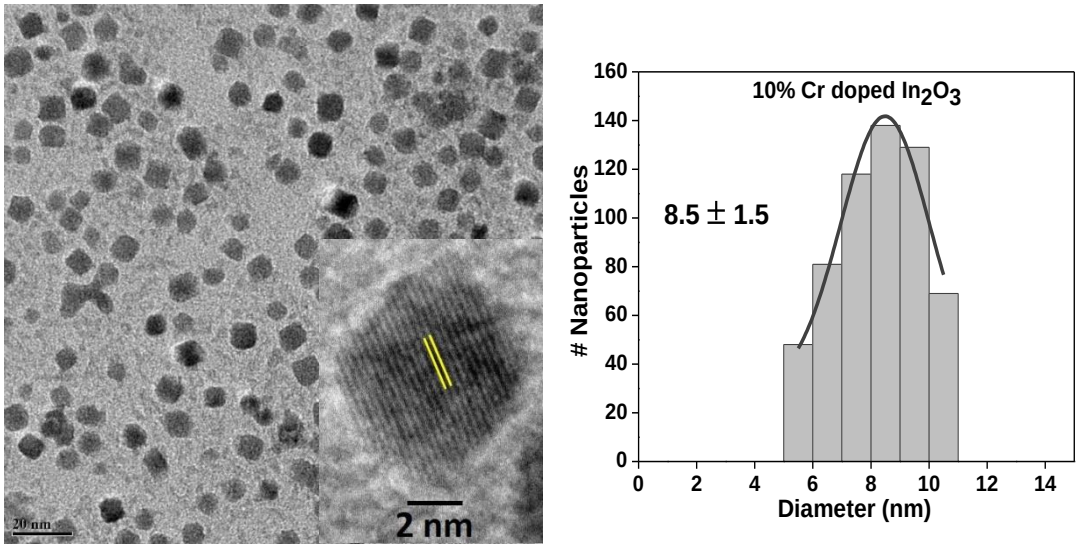

Figure 14: TEM image for 10% Cr doped In_2O_3 NCs with size histogram. Inset shows HRTEM image.

Inset in figure 14 and figure 15(a), (b) and (c) are High Resolution TEM (HRTEM) images. HRTEM shows interplanar distance of ~2.5 Å for all the Cr-Sn codoped and Cr doped NCs corresponding to (400) plane which agrees well with the XRD (using Braggs Equation) results shown in table 3.

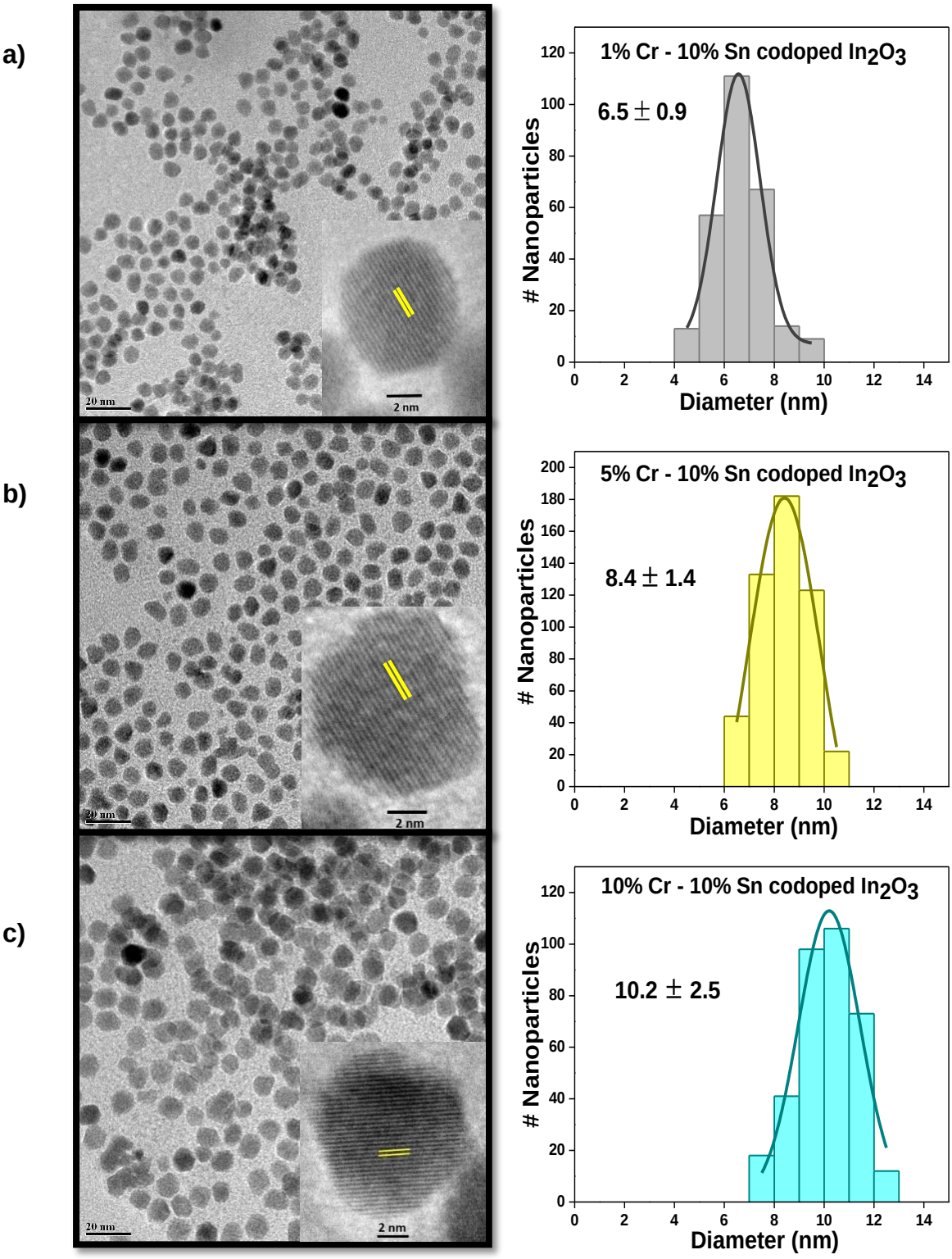

Figure 15: TEM image of %Cr-10% Sn codoped In_2O_3 NCs. a) 1% Cr, b) 5% Cr, c)10% Cr with respective size histograms. Inset shows HRTEM of respective samples.

3.2.3. Electron Paramagnetic Resonance (EPR)

Figure 16 shows X-band EPR spectra at 9.45 GHz in the magnetic field range of 2500G – 4250G at 300K for (a) Cr-doped and (b) Cr-Sn codoped In_2O_3 NCs. Cr^{3+}, a d^3 electronic configuration ion with 3 unpaired electrons and Spin value of 3/2 has 2 Kramer's doublets: ±3/2 and ±1/2, which can give rise to 4 hyperfine lines. However for Cr, nuclear spin I=0, so there are no hyperfine interactions between Cr nucleus and the free electrons, hence no hyperfine splitting.[18] In the obtained EPR spectra, there was no sign of hyperfine splitting, which confirms the presence of Cr ion. Furthermore, Lande g factor was calculated for both the spectra. The EPR spectra exhibited a broad signal centered at g value of 1.99 and 1.994 for Cr doped and Cr-Sn codoped NCs respectively. The g-factor values are in good correlation with the prior literature where g=1.99 to 2.00 has been assigned to presence of Cr^{3+} ions in octahedral environment.[27-28] EPR result confirms the presence of Cr in 3+ oxidation state in both Cr doped and Cr-Sn codoped In_2O_3 NCs.

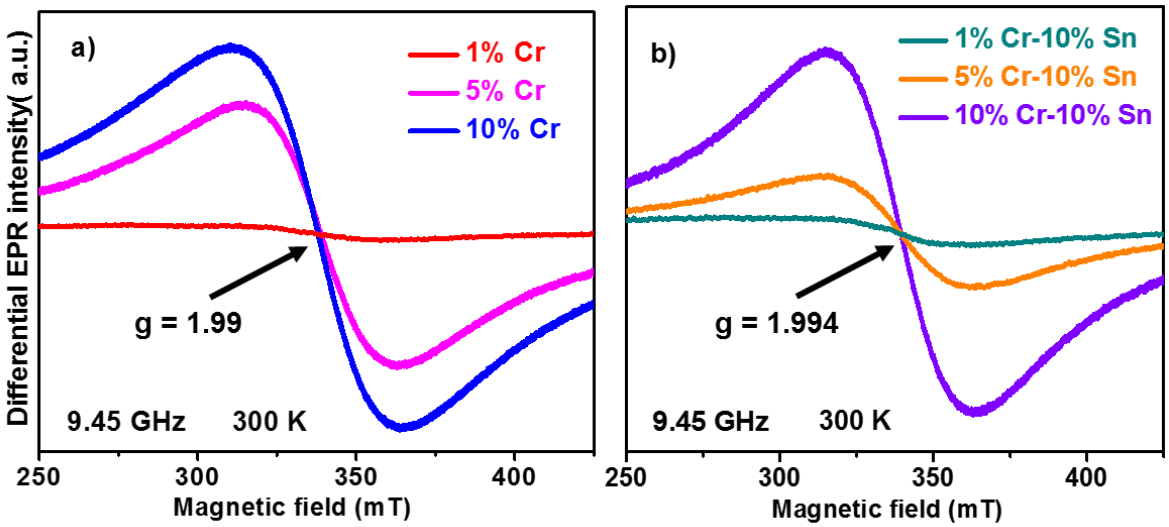

Figure 16: EPR spectra for a) Cr doped In_2O_3 NCs. b) Cr-Sn codoped In_2O_3 NCs.

3.2.4. UV-visible-Near Infrared Absorption

Cr-Sn codoped In_2O_3 NCs show strong absorption peak in near to mid infrared region (figure 17). 10% Sn doped In_2O_3 NCs exhibits localized surface plasmon resonance (LSPR) band at 2298nm (0.539 eV). Also there is an additional peak (optical band gap) in the UV region for all the Cr-Sn codoped NCs. This additional band provides optical

transparency in the visible region. The optical band gap decreases with increase in Cr doping which can be rationalized by the sp-d exchange interaction.[25]

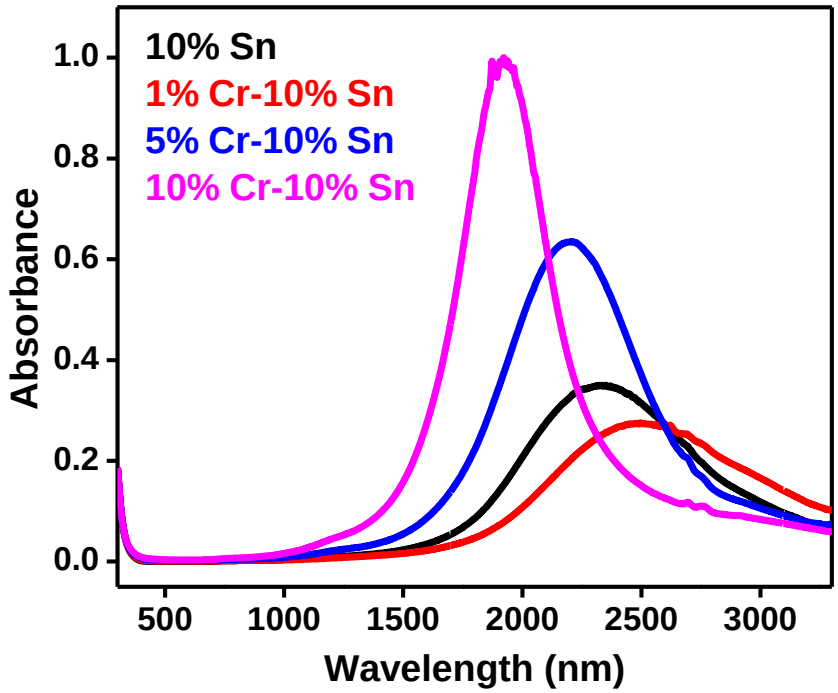

Figure 17: Variation of LSPR band in near to mid IR region for Cr-Sn codoped In_2O_3 NCs.

On codoping10% Sn with Cr, initially (at 1% Cr concentration), LSPR band red shifts and becomes less intense w.r.t 10% Sn, but on further increase in amount of Cr doping (5% Cr and 10% Cr), LSPR band becomes more intense and blue shifts to lower wavelengths as compared to 10% Sn.doped In_2O_3 NCs. This near IR plasmonic behavior is unusual because in other reported transition metal (Fe and Mn) and Sn codoped NCs, LSPR band red shifts with codoping of T.M. with Sn, and vanishes at higher T.M. dopant concentrations.[8-9] Also Cr-Sn codoped In_2O_3 NCs showing plasmonic properties are reported for the first time here.

LSPR depends on several factors like size, shape, refractive index of the medium, material and most importantly charge carrier concentration.[1] All the factors other than size and carrier density remain same for all the NCs. In Cr-Sn codoped NCs, size is increasing with increase in Cr doping as shown by TEM, according to which LSPR band should red shift towards longer wavelength.[1] However, it is blue shifting towards lower wavelengths,

which may be due to dominance of other factors like carrier density, which might be increasing with increase in Cr doping.

The shift of plasmonic band to lower wavelengths is not known but might be explained by the following hypothesis:

1.) On doping of Sn^{4+} in In_2O_3 lattice, Sn forms a complex $(\boldsymbol{O_i''2Sn_{In}^{\cdot}})^{x}$ which slowly generates free electrons based on the following equilibrium reaction.[9, 29]

$$(\boldsymbol{O_i''2Sn_{In}^{\cdot}})^{x} \leftrightarrow \boldsymbol{2Sn_{In}^{\cdot}} + \boldsymbol{2e'} + \frac{\boldsymbol{1}}{\boldsymbol{2}}\boldsymbol{O_2}$$

Where $\boldsymbol{Sn_{In}^{\cdot}}$ is a positively charged Sn on an In site and $\boldsymbol{O_i''}$ is an interstitial oxygen having -2 charge. On codoping with Cr, maybe the stability of complex is decreasing and decomposes more easily to give free electrons. In other words, equilibrium is more favourable towards forward direction in presence of Cr, thereby increasing electron density.

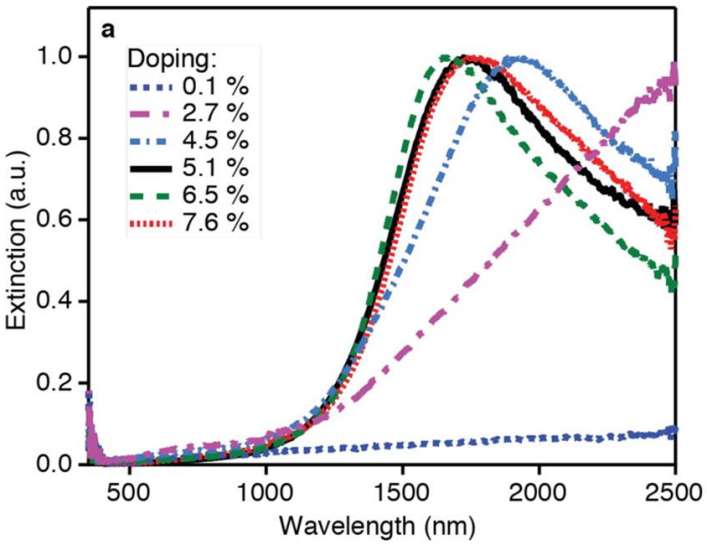

Figure 18: Variation of LSPR band with change in Sn dopant concentration in Sn doped In_2O_3 NCs (adapted from reference 30 with permission of ACS).

2.) Recently, Milliron et al.[30] demonstrated that the distribution of Sn dopant ions also plays major role in the LSPR band. They showed that Sn dopant ions which are doped on the surface of the NCs exhibit narrower LSPR band compared to the Sn dopant ions doped in the core of the In_2O_3 NC lattice. In Figure 18 (adapted from reference 30) for Sn doped In_2O_3 NCs, it has been shown that from 0.1% to 5.1%, there is blue shift in LSPR,

and at higher concentrations (6-7.6%), there is not much change. Also it has been shown that Sn doping shows uniform dopant distribution for low doping levels and surface segregation of tin at higher doping levels. Between 4.5 and 5.1 %, there is not much difference in dopant concentrations, but still there is significant shift (~300nm) in LSPR band. This is because in case of 5.1% more tin is doped on the surface, which easily activates to give more free electrons. So, the possible hypothesis for blue shift in LSPR band of Cr-Sn is such that, with increase in Cr concentration may be more number of Sn dopants are doped on the surface of the NCs, rather than in the core.[30]

3.2.5. Electrical DC Measurements

In order to find the reason behind the shift in LSPR, four probe DC electrical conductivity measurements were done for Cr-Sn codoped NCs on solid pellets. Resistivity versus temperature graph (Figure 19) shows typical non-metallic behavior. It is clearly evident from the graph that, on codoping with 1% Cr, initially resistivity increases as compared to 10% Sn doped IO NCs, but on further increasing Cr dopant concentration to 5% and 10%, resistivity decreases systematically, but it is still larger than 10% Sn In_2O_3 NCs.

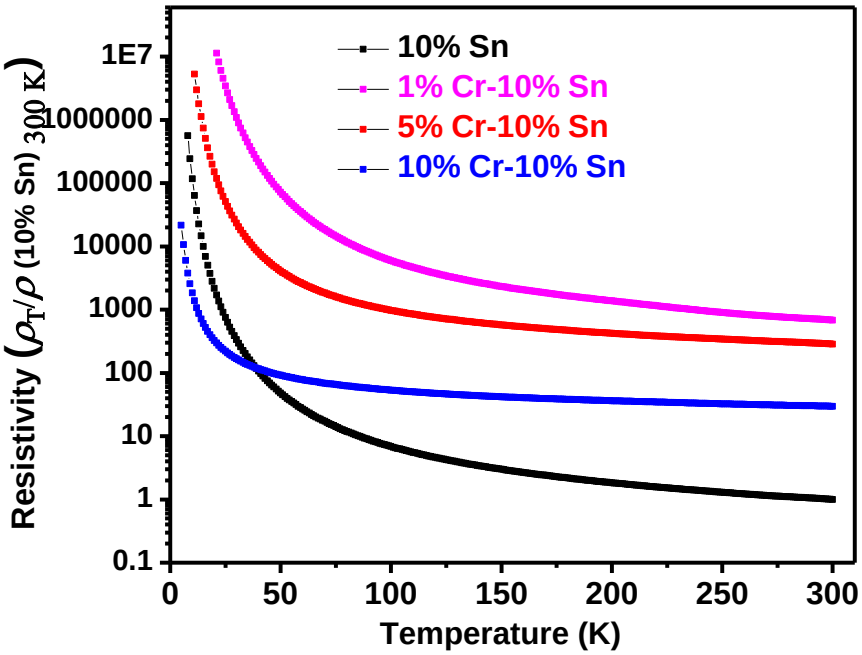

Figure 19: Temperature dependent resistivity plot for Cr-Sn codoped In_2O_3 NCs where ρ_T is resistivity at any temperature T for all the samples and $\rho(10\%\ Sn)_{300K}$ is resistivity of 10% Sn doped In_2O_3 NCs at 300K. (Y-axis is in log scale for comparison).

At room temperature, conductivity was measured for all the samples. DC Conductivity is maximum for 10% Sn doped NCs, followed by 10% Cr -10% Sn, 5% Cr-10% Sn and 1% Cr-10% Sn codoped NCs. This trend is partially similar to LSPR trend where initially on 1% Cr codoping, LSPR red shifts and at higher Cr concentrations (5% and 10%), it blue shifts. This may be because conductivity also depends on other factors like mobility.

3.2.6. Magnetism

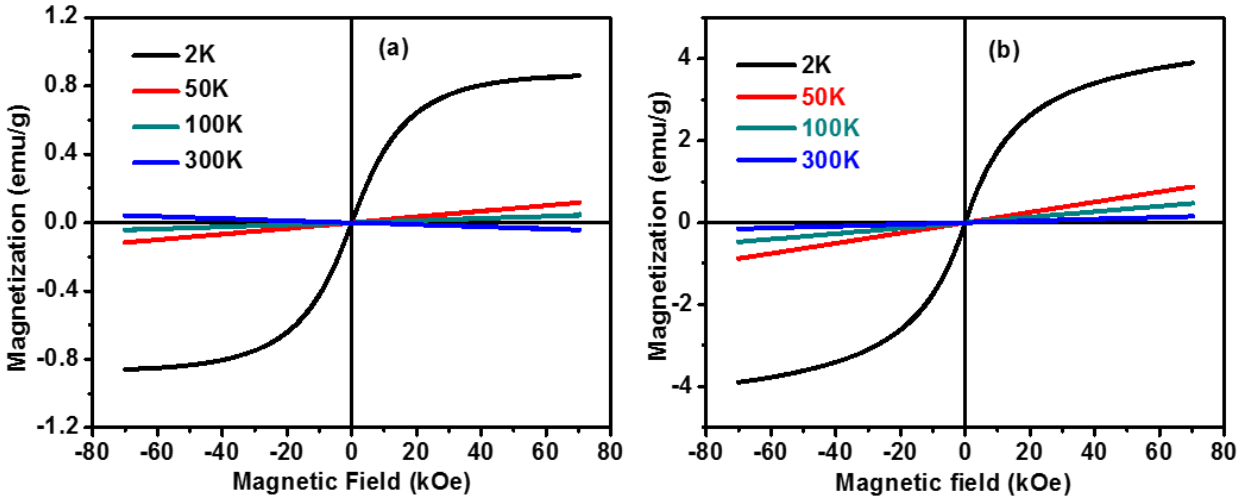

Figure 20: Magnetization vs magnetic field strength curves for a) 10% Cr doped In_2O_3 NCs b) 1% Cr doped In_2O_3 NCs at different temperatures.

Magnetic measurements have been done only for Cr doped In_2O_3 NCs shown in figure 20. Both10% Cr and 1% Cr doped In_2O_3 NCs are also found to be of paramagnetic nature exhibiting no hysteresis and zero coercivity (figure 20a and 20b). There is complete overlap between ZFC and FC curves at all temperatures for both the samples (1% Cr-10% Sn is shown in figure 21). This is in accordance with theoretical studies done by Zunger et al.[10-11] where only Cr doped In_2O_3 NCs were predicted to show paramagnetic nature. The magnetic moment per Cr ion was calculated and it was found to be 0.986 μ_B for 10% Cr doped In_2O_3 NCs and 2.66 μ_B for 1% Cr doped In_2O_3 NCs. The decrease in magnetic moment/Cr on increase in Cr dopant concentration is due to more antiferromagnetic interaction between Cr spins as spins are in more close proximity in case of 10% Cr doped NCs. The value of magnetic moment of 1% Cr doped sample is more as compared to the values reported in literature for Cr doped In_2O_3 films. [31-32]

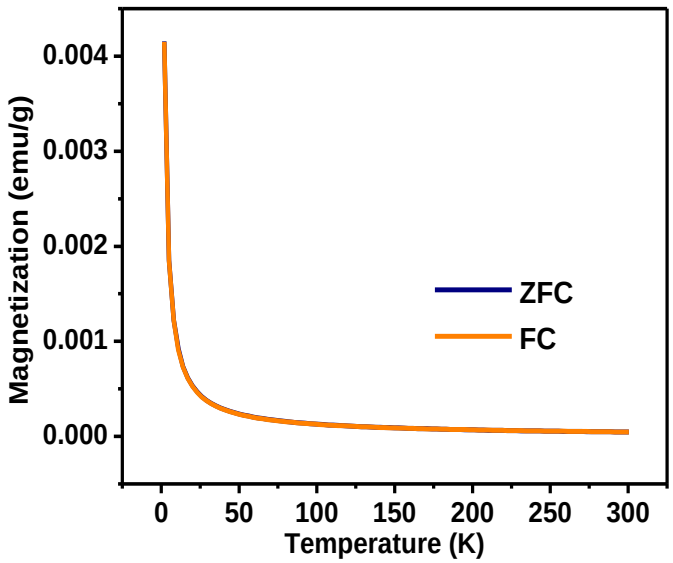

Figure 21: Variation in magnetization with temperature curve for 10% Cr doped In_2O_3 NCs under (zero field cooled and field cooled, 100 Oe) conditions.

4. Conclusions

Colloidal Mn-Sn and Cr-Sn codoped In_2O_3 NCs have been reported for the first time. Concentration of each dopant ions were varied in the range of 0-10% and size of NCs were in the range of 7-11 nm, mostly with spherical morphology. Though Mn^{3+} doping were attempted using Mn^{3+} precursor, characterization of product NCs showed doping of Mn^{2+} in both Mn-doped In_2O_3 and Mn-Sn codoped In_2O_3 NCs. Q-band EPR data showed the clear sextet hyperfine splitting corresponding Mn^{2+} ion in the product NCs. Essentially, Mn^{3+} get converted to Mn^{2+} after accumulating an electron from oxygen vacancies and/or Sn^{4+} doping. This trapping of electrons by localized Mn *d*-states located in the deep in mid-gap also influences the LSPR and electrical conductivity, where LSPR peak shifts toward higher energy and conductivity decreases with increasing Mn content in Mn-Sn codoped NCs.

Above results motivated to synthesize colloidal Cr-Sn codoped In_2O_3 NCs since prior theoretical calculations suggested unoccupied Cr^{3+} *d*-level lies above the conduction band minimum of In_2O_3, unlike the deep mid-gap Mn *d* trap states. Based on this theoretical prediction, LSPR and electrical conductivity should not get perturbed much with Cr doping, unlike the case of Mn doping where carrier density decreases drastically with increasing Mn concentration. To our surprise, LSPR band shifts toward higher energy along with an increase in electrical conductivity by increasing the Cr concentration from 1-10% in Cr-Sn codoped In_2O_3 NCs. Even though the exact reason behind this phenomenon is unclear at present, plausible reasons behind these observation has been discussed in the literature. Magnetic data of both Cr doped In_2O_3 NCs and Mn-Sn codoped In_2O_3 NCs were found to be of paramagnetic nature. However, preliminary data showing effect of Sn codoping on magnetic properties suggest the possibility of carrier mediated magnetic coupling, which will be studied further in future.

5. References

1. Luther, J. M.; Jain, P. K.; Ewers, T.; Alivisatos, A. P. Localized surface plasmon resonances arising from free carriers in doped quantum dots. *Nat. Mater.* ***2011*****,** *10*, 361-366.

2. Alvarez, M. M. *et al*. Optical absorption spectra of nanocrystal gold molecules. *J. Phys. Chem. B,* **1997**, *101*, 3706–3712 ()

3. Pérez-Juste, J., Pastoriza-Santos, I., Liz-Marzán, L. M. & Mulvaney, P. Gold nanorods: Synthesis, characterization and applications. *Coord. Chem. Rev.* **2005**, *249*, 1870–1901.

4. Bounsanti, R; Milliron D. J. Chemistry of Doped Colloidal Nanocrystals. *Chem. Mater.* **2013**, *25*, 1305-1317.

5. Radovanovic, P. V. Nanowires: Keeping track of dopants. *Nat. Nanotechnol*. **2009**, 4, 282-283.

6. Kanhera, M.; Koike, H.; Yoshinaga, T.; Teranishi, T. Indium tin oxide nanoparticles with compositionally tunable surface plasmon resonance frequencies in the near-IR region. *J. Am. Chem. Soc*., **2009**, *131*, 17736-17737.

7. Comin, A.; Manna, L. New materials for tunable plasmonic colloidal nanocrystals. *Chem. Soc. Rev.* **2014**, *43*, 3957-3975.

8. Tandon, B.; Shanker, G. S.; Nag, A. Multifunctional Sn- and Fe-Codoped In2O3 Colloidal Nanocrystals: Plasmonics and Magnetism. *J. Phys. Chem. Lett.* **2014,** *5*, 2306-2311.

9. Shanker, G. S.; Tandon, B.; Shibata, T.; Chattopadhyay, S.; Nag, A. Doping Controls Plasmonics, Electrical Conductivity, and Carrier-Mediated Magnetic Coupling in Fe and Sn Codoped In2O3 Nanocrystals: Local Structure Is the Key. *Chem. Mater.* **2015,** *27*, 892-900.

10. Raebiger, H.; Lany, S.; Zunger, A. Electronic structure, donor and acceptor transitions, and magnetism of 3d impurities in In_2O_3 and ZnO. *Phys. Rev. B* **2009**, *79*, 165202.

11. Raebiger, H.; Lany, S.; Zunger, A. Control of Ferromagnetism via Electron Doping in In_2O_3:Cr. *Phys. Rev. Lett*. **2008**, *101*, 027203.

12. Shannon, R. D.; Prewitt, C.T.; Effective ionic radii in oxides and flourides. *Acta Crystallogr. B*. **1969**, *25*, 925-945.

13. Farvid, S. S.; Sabergharesou, T.; Hutfluss, L. N.; Hegde, M.; Prouzet, E.; and Radovanovic, P. V. Evidence of Charge-Transfer Ferromagnetism in Transparent Diluted Magnetic Oxide Nanocrystals: Switching the Mechanism of Magnetic Interactions. *J. Am. Chem. Soc.* **2014**, 136, 7669-7679.

14. An, Y.; Wang, S.; Duan, L.; Liu, J.; Wu, Z. Local Mn structure and room temperature ferromagnetism in Mn-doped In_2O_3 films. *Appl. Phys. Lett*. **2013**,102, 212411.

15. Gilstrap, R. A.; Capozzi, C. J.; Carson, C. G.; Gerhardt, R. A.; Summers, C. J. Synthesis of a Nonagglomerated Indium Tin Oxide Nanoparticle Dispersion. *Adv. Mater.* **2008**, *20*, 4163.

16. Zimmerman, J. Physical Chemistry for the biosciences: Chang, Raymond. *Biochem. Mol. Biol. Edu.* **2005**, *33*, 382.

17. Warschkow, O.; Ellis, D. E.; Gonzalez, G. B.; Mason, T. O. Defect Structures of Tin-Doped Indium Oxide. *J. Am. Ceram. Soc*. **2003**, *86*, 1700.

18. Krzystek, J.; Ozarowski, A.; Telser, J. Multi-frequency, high-field EPR as a powerful tool to accurately determine zerofield splitting in high-spin transition metal coordination complexes. *Coord. Chem. Rev.* **2006**, *250*, 2308-2324.

19. Matumura, O. Electron Spin Resonance of Mn-activated Phosphors. Journal of the Physical Society of Japan 1959, 14, 108-108

20. Norberg, N. S.; Kittilstved, K. R.; Amonette, J. E.; Kukkadapu, R. K.; Schwartz, D. A.; Gamelin, D. R. Synthesis of colloidal Mn^{2+}: ZnO quantum dots and high-Tc ferromagnetic nanocrystalline thin films. *J. Am. Chem. Soc.* **2004,** *126*, 9387-9398.

21. Sarma, D. D.; Jagadeeswararao, M.; Pal, S.; Nag, A. Electrical and Plasmonic Properties of Ligand-Free Sn^{4+}-Doped In_2O_3 (ITO) Nanocrystals. *ChemPhysChem* **2016**, DOI: 10.1002/cphc.201500973.

22. Irvine, J. T. S.; Sinclair, D. C.; West, A. R. Electroceramics: Characterization by Impedance Spectroscopy. *Adv. Mater.***1990,** *2*, 132-138.

23. Wang, T.; Radovanovic, P. V. Free Electron Concentration in Colloidal Indium Tin Oxide Nanocrystals Determined by Their Size and Structure. *J. Phys. Chem. C* **2011,** *115*, 406-413.

24. Schimpf, A. M.; Lounis, S. D.; Runnerstrom, E. L.; Milliron, D. J.; Gamelin, D. R. Redox Chemistries and Plasmon Energies of Photodoped In_2O_3 and Sn-Doped In_2O_3 (ITO) Nanocrystals. *J. Am. Chem. Soc.* **2015,** *137*, 518-524.

25. Wang, X. L.; Luan, C. Y.; Shao, Q.; Pruna, A.; Leung, C. W.; Lortz, R.; Zapien, J. A.; Ruotolo, A. Effect of the magnetic order on the room-temperature band-gap of Mn-doped ZnO thin films. *Appl. Phys. Lett*. **2013**, *102*, 102112.

26. Farvid, S.S.; Ju, L.; Worden, M.; Radovanovic, P. V. Colloidal chromium-doped In_2O_3 nanocrystals as building blocks for high-Tc ferromagnetic transparent conducting oxide structures. *J. Phys. Chem. C*. **2008,** *112*, 17755-17759.

27. Yamaga, M.; Tsuzuki, H.; Takeno, S.; Villora, E. G.; Shimamura, K. Electron-spin resonance of transparent conductive oxide β-Ga_2O_3. *J. Non-Cryst. Solids* **2012**, *358*, 2458-2461.

28. Prathima, B.; Rao, Y. S.; Chalapathi, P.V.; Reddy, Y. P.; Reddy, V. Spectral, structural and biological analysis of Cr(III) complex with benzyloxybenzaldehyde-4-phenyl-3-Thiosemicarbazone. *Int. J. Pharm. Pharm. Sci.* **2012**, *4*, 167-174.

29. Gonzalez, G. B. Investigating the Defect Structures in Transparent Conducting Oxides Using X-Ray and Neutron Scattering Techniques. *Materials* **2012**, *5*, 818-850.

30. Lounis, S. D.; Runnerstorm, E. L.; Bergerud, A.; Nordlund, D.; Milliron, D. J. Influence of Dopant Distribution on the Plasmonic Properties of Indium Tin Oxide Nanocrystals. *J. Am. Chem. Soc.* **2014**, *136*, 7110-7116.

31. Farvid, S. S.; Ju, L.; Worden, M.; Radovanovic, P. V. Colloidal Chromium-Doped In_2O_3 Nanocrystals as Building Blocks for High-T_C Ferromagnetic Transparent Conducting Oxide Structures. *J. Phys. Chem. C*, **2008**, *112*, 17755-17759.

32. Philip, J.; Punnoose, A.; Kim, B. I.; Reddy, K. M.; Layne, S.; Holmes, J. O.; Satpati, B.; LeClair, P. R.; Santos, T. S.; Moodera, J. S. Carrier-controlled ferromagnetism in transparent oxide semiconductors. *Nat. Mater.* **2006**, *5*, 298-304.